fluids

MDPI

Article

Improving Homogeneity of 3D-Printed Cementitious Material Distribution for Radial Toolpath

Mingyang Li [1], Zhixin Liu [2], Jin Yao Ho [1] and Teck Neng Wong [1,*]

[1] Singapore Centre for 3D Printing, School of Mechanical & Aerospace Engineering, Nanyang Technological University, 50 Nanyang Avenue, Singapore 639798, Singapore
[2] China Aerospace Times Feihong Technology Corperation Limited, Beijing 100854, China
* Correspondence: mtnwong@ntu.edu.sg

Abstract: The 3D cementitious material printing method is an extrusion-based additive manufacturing strategy in which cementitious materials are extruded through a dynamic nozzle system to form filaments. Despite its ability to fabricate structures with high complexity and efficiency, the uneven material distribution during the extrusion and deposition process is often encountered when a radial toolpath is introduced. This limits the design freedom and printing parameters that can be utilized during radial toolpath printing. Here, we report a facile strategy to overcome the existing challenges of cementitious material non-homogeneity by rationally developing new nozzle geometries that passively compensate the differential deposition rate encountered in conventional rectangular nozzles. Using two-phase numerical study, we showed that our strategy has the potential of achieving a homogeneous mass distribution even when the nozzle travel speed is unfavorably high, while filament from a rectangular nozzle remains highly non-homogenous. The material distribution unevenness can be reduced from 1.35 to 1.23 and to 0.98 after adopting trapezoid and gaussian nozzles, indicating improvements of 34.3% and 94.2%, respectively. This work not only outlines the methodology for improving the quality of corner/curved features in 3DCMP, but also introduces a new strategy which can be adopted for other extrusion-based fabrication techniques with high material inertia.

Keywords: additive manufacturing; cementitious materials; non-Newtonian fluid; two-phase flow; numerical modeling; nozzles

Citation: Li, M.; Liu, Z.; Ho, J.Y.; Wong, T.N. Improving Homogeneity of 3D-Printed Cementitious Material Distribution for Radial Toolpath. *Fluids* **2023**, *8*, 87. https://doi.org/10.3390/fluids8030087

Academic Editors: Chengcheng Tao and Mehrdad Massoudi

Received: 23 January 2023
Revised: 17 February 2023
Accepted: 25 February 2023
Published: 1 March 2023

1. Introduction

The 3D cementitious material printing (3DCMP) method has gained significant traction in the past few years due to its ability to fabricate complex yet functional structures. Its autonomous fabrication process, which reduces reliance on manual labor and improves construction safety, is also a unique feature which makes 3DCMP technology appealing to the building industry [1–4]. Most existing 3DCMP systems utilize an extrusion-based additive manufacturing (AM) strategy in which fresh cementitious materials are extruded through a dynamic nozzle system to form filaments. The filaments are then deposited layer-by-layer to produce three-dimensional parts. During the fabrication process, cementitious material experiences high stresses as it is squeezed through the nozzle. These stresses are instantaneously released at the nozzle exit, resulting in material outward expansion and mass redistribution within the filament during deposition [5]. To this end, the mass distribution homogeneity of the cementitious filaments during deposition plays a pivotal role, as it not only affects the bulk structural properties of finished products but also prevents skewing and tearing of extrudates due to deposition differences [6].

Unfortunately, uneven material distribution is often encountered when the nozzle movement deviates from a straight line, i.e., when a radial toolpath is introduced. A radial toolpath is commonly used to produce corner features and surface curvatures [7] and is an

attractive feature of 3DCMP, which enables the fabrication of intricate products. However, owing to the cementitious material inertia, as the nozzle negotiates a turn, a difference in deposition rate arises between the segment of the filament nearest to the center of the turning radius and the segment furthest away [8]. This variation in deposition rate, and, hence, material distribution non-homogeneity across the filament, can be further intensified when smaller toolpath radius, higher nozzle travel speed, and larger filament width are employed [8]. This undesirable effect limits the design freedom and printing parameters that can be utilized during radial toolpath printing. Furthermore, despite recent exhaustive efforts in optimizing the rheological properties of the materials, such as plastic viscosity (k) and yield stress (τ_0), and printing parameters, such as relative nozzle travel speed (ξ) and nozzle aspect ratio (φ) [8–10], the material mass distribution ratio (ϕ) (a parameter which characterizes the homogeneity of a deposited filament, with $\phi = 1$ indicating a uniform mass distribution and a non-uniform distribution when ϕ deviates from 1) lower than 1.25 cannot be achieved with the commonly used rectangular-shaped nozzle when the toolpath radius (R) is small, i.e., $\leq$30 mm [8].

In this paper, we report a facile strategy to overcome the existing challenges of cementitious material non-homogeneity for a small toolpath radius by rationally developing new nozzle geometries that passively compensate for the undesirable differential deposition rate encountered in conventional rectangular nozzles. Using R = 30 mm as a demonstration framework, we numerically showed that our strategy has the potential of achieving ϕ close to 1 even when the nozzle travel speed is unfavorably high, while the filament deposited by a rectangular nozzle remains highly non-homogenous. This work not only outlines the methodology for improving the quality of corner and curved features in 3DCMP, but also introduces a new strategy which can be adopted for other extrusion-based fabrication techniques with high material inertia [11,12].

2. Method

Since observing the details inside the cementitious material flow is difficult, CFD simulations are used to study the characteristics of cementitious material flow under various conditions [13]. To track the interface between the concrete paste and air, the volume of fluid (VOF) is adopted to simulate the concrete flow and the deposition process. The governing equations of the VOF formulations on multiphase flow are shown as follows.

The continuity equation is as follows:

$$\frac{\partial \rho}{\partial t} + \nabla \cdot \left(\rho \vec{v}\right) = 0 \tag{1}$$

The equation of momentum is as follows:

$$\frac{\partial \left(\rho \vec{v}\right)}{\partial t} + \nabla \cdot \left(\rho \vec{v} \vec{v}\right) = \nabla p + \nabla \cdot \tau + \rho g \tag{2}$$

The volume fraction equation is as follows:

$$\frac{\partial \alpha_m}{\partial t} + \vec{v} \cdot \nabla \alpha_m = 0 \tag{3}$$

$$\tau = \tau_0 + k\dot{\gamma} \tag{4}$$

where $\rho = \alpha_c \rho_c + \alpha_a \rho_a$ and $k = \alpha_c k_c + \alpha_a k_a$, α_m is the volume fraction of the m-th fluid in the system, $\dot{\gamma}$ (s^{-1}) is the shear rate, τ_0 (Pa) is the yield stress, and ρ_c (kg/m^3) and ρ_a (kg/m^3) are the density of the concrete paste and air, respectively; k_c (Pa·s) is the plastic viscosity of concrete paste, and k_a (Pa·s) is the dynamic viscosity of air.

The simulation domain is shown in Figure 1. It is composed of a vertical inlet zone and a horizontal deposit zone. Depending on the investigated nozzle shape, the vertical inlet zone is meshed with approximately 31 radial points, 21 angular points, and 31 vertical

points. The horizontal deposit zone is meshed with 161 angular points, 46 concentric circles, and 21 vertical points. The largest cell size is smaller than 1 mm^3. The node number of the mesh is 175,707 when the mesh independence is reached. A stream of cementitious material is fed into the inlet zone, which then flows into the deposit zone. The ANSYS FLUENT 2022 R1 commercial software (ANSYS, Inc., Canonsburg, PA, USA) was used to perform the numerical simulation. The model geometry was meshed with the preprocessor ICEM CFD 2022 R1 software (ANSYS, Inc., Canonsburg, PA, USA) and imported to ANSYS FLUENT 2022 R1. A segregated time-dependent solver was used. The uniform inlet velocity of the concrete paste was applied, and the outlet is atmospheric pressure. The PRESTO software was selected for the pressure interpolation, and the PISO was selected for pressure–velocity coupling. A second-order up-wind differentiating scheme is used for differentiating the momentum equation. The implicit body force treatment was implemented for body force formulation. In addition, the time scale was set as $\Delta t = 5 \times 10^{-4}$ s, and the relaxation factor was adjusted to ensure convergence. Details of the simulation procedures are reported in the authors' previous work [8].

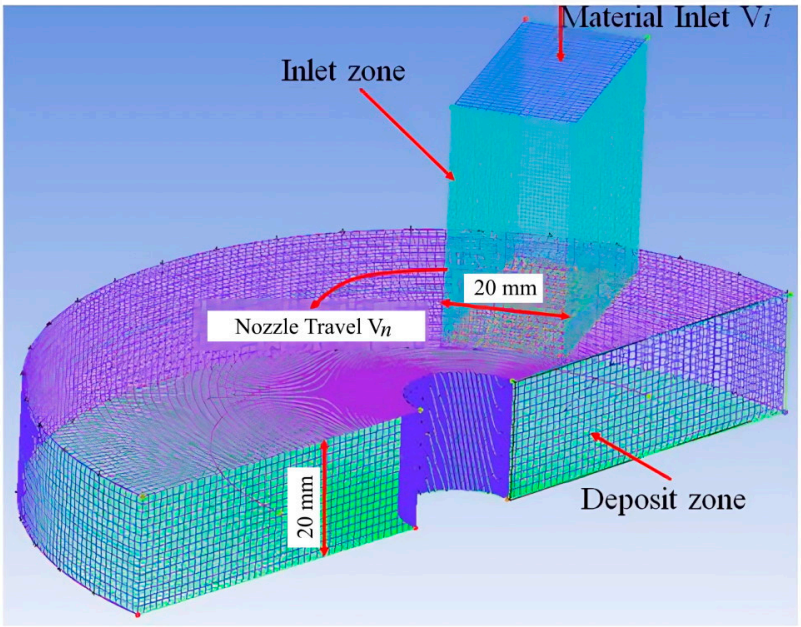

Figure 1. Exemplary simulation domain of cementitious material extrusion and deposition of 3DCMP with radial toolpath. Image extracted from Ref. [8].

An exemplary result of the extrusion and deposition process of the cementitious material with a radial toolpath is depicted in Figure 2. It should be noted that in the simulation, the nozzle only commenced its motion after the initial extruded material was deposited. This process was deliberately modelled so that the influence of the initial deposit process on the mass distribution of the printed material at corners could be eliminated. The simulation was terminated when the deposition process time lasted for approximately 2 s. As shown in Figure 2, material mass distribution ratio (ϕ) refers to the ratio of the inner side cross-section area (S_i) that is close to the corner center to the outer side cross-section area of the printed filament (S_o), i.e., $\phi = S_i/S_o$. In this study, ϕ is evaluated at the plane where the material was deposited for nearly 1.5 s so that the effect of deposition time has no influence on the mass distribution of the printed filament.

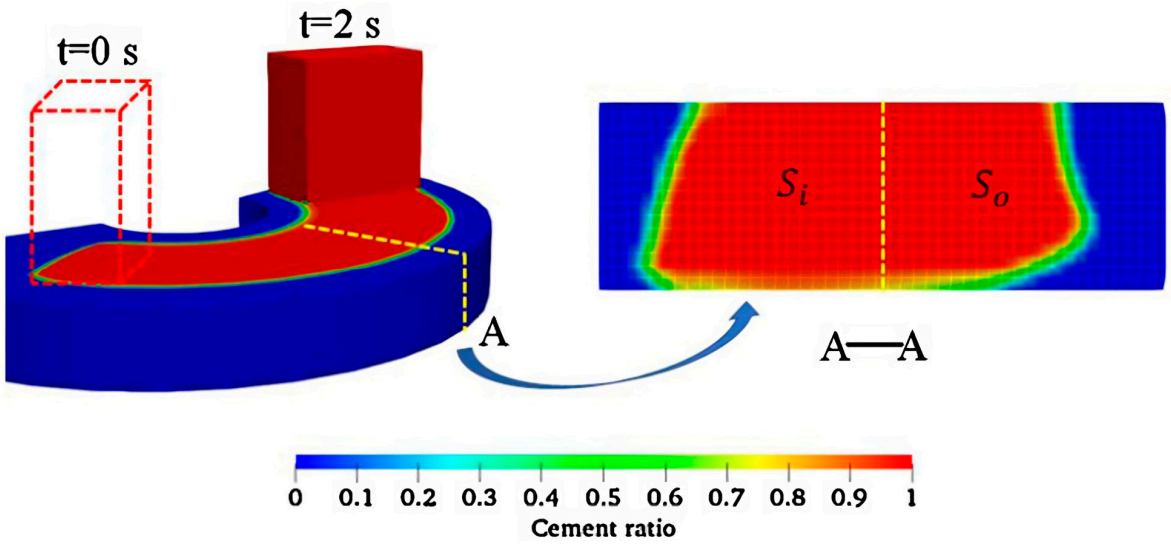

Figure 2. Example of simulation result. Cross-section A-A illustrating inner side (S_i) and outer side (S_o) cross-sectional area of a filament extracted from Ref. [8].

3. Results and Discussion

To demonstrate the influence of radial toolpath on material mass distribution, a time-dependent numerical simulation of the cementitious material extrusion and deposition process in ambient air was performed. It should be emphasized that, in order to validate the accuracy of our 3D simulation model, the simulation results obtained from our model were compared against the experimental results. The detailed comparisons are reported in Ref. [8], and the pictorial comparisons are extracted as Figure 3. In Figure 3a, the material used in the experiment is composed of cement (OPC, CEM I 42.5, EnGro), fine sand, fly ash (Class F, Jaycee), and silica fume (Microsilica Grade 940, Elkem). To ensure the homogeneity of the cementitious mixture, the mixing process was carried out by firstly dry mixing all of the powder ingredients at 18 rpm for 3 min. This was then followed by the remixing of water with superplasticizer and adding them to the cement mixture. This mixing procedure lasts about 1 min at 33 rpm, followed by 2 min at 61 and 113 rpm each. Finally, the fresh cementitious material is further mixed for 1 min at 61 rpm. The aforementioned mixing procedures were developed from our past studies in which rheological test conducted demonstrated good homogeneity to a millimeter length scale [10]. The properties of the cementitious materials, which are also used in the simulations in this study, were measured and listed in Table 1. As shown in Figure 3, the simulation results fit well with the experimental results, indicating that the proposed 3D simulation model can be used to study the material distribution in the 3DCP process.

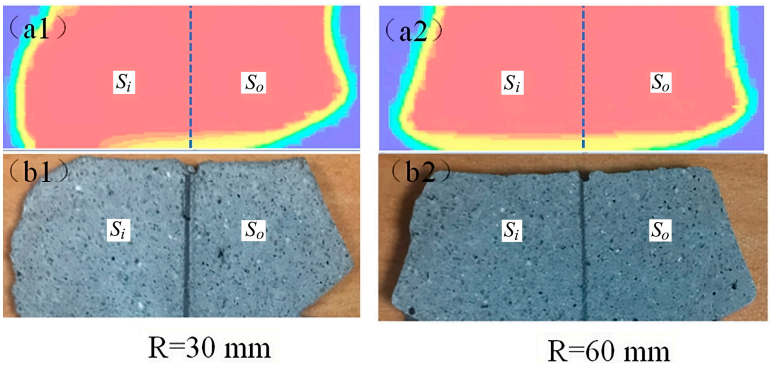

Figure 3. Numerical simulation and experimental results of the cross-section of the printed filament at corners, with (**a**) simulation results and (**b**) experimental results [8].

Table 1. Material properties measured and used in simulations.

Property	Density (kg/m^3)	Yield Stress (Pa)	Plastic Viscosity (Pa·s)
Value	2200	516	6.5

Figure 4 shows the material mass distribution of the filament cross-section during deposition. Here, the simulation was performed with a constant R value of 30 mm and the rectangular nozzle of $\varphi = 2$, which corresponds to the nozzle length (L) of 30 mm and width (W) of 15 mm. In order to reduce the fabrication time while improving the surface finishing of construction scale printings, rectangular nozzles are implemented in 3DCMP to fabricate rectangular filaments to compose smooth straight walls. In this study, the low R and high φ values were rationally selected, as they represent a more stringent condition in which a high degree of non-homogeneity in the filament occurs during deposition. While maintaining these two parameters, ξ ranged between 1.00 and 1.10. It should also be emphasized that ξ denotes the ratio of material velocity as it exits the nozzle (V_i) to the nozzle tangential velocity (V_n). Hence, with a constant V_i, a larger ξ value denotes a lower V_n.

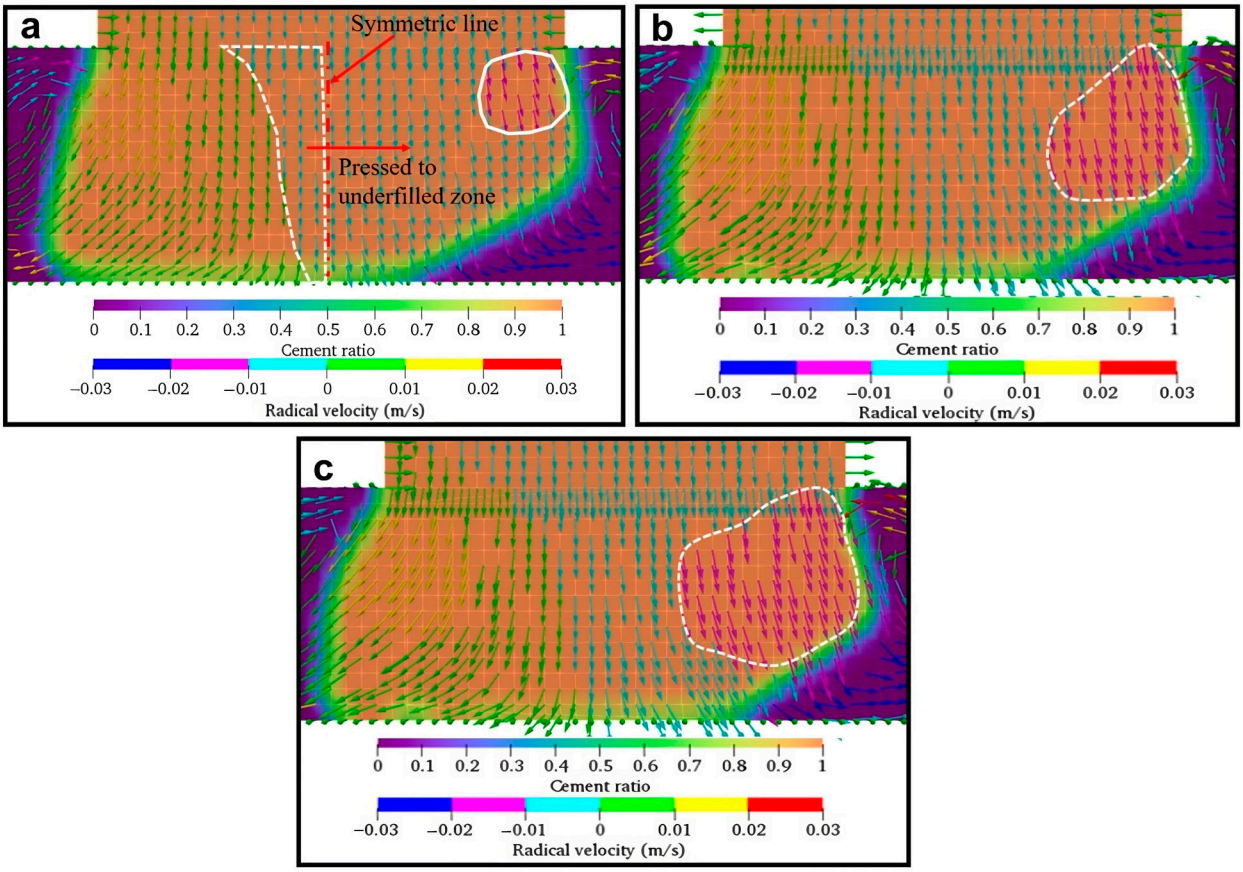

Figure 4. Cement ratio and velocity vector using rectangular nozzle, $\varphi = 2$, $R = 30$ mm, and ζ of (**a**) 1.00, (**b**) 1.05, and (**c**) 1.10.

It can be seen from Figure 4 that the mass distribution of the deposited filament is highly non-homogeneous. For all ξ values, the mass distribution is skewed towards the left (or towards the center of the radial toolpath) where more material is deposited, which is very different comparing to the material which just comes out from a rectangular nozzle [14]. On the contrary, on the right segment of the filament (or segment of the filament further away from the center of the radial toolpath), there exists an empty space that is not occupied by the material. This left-side bias deposition of material is mainly due to the presence of centripetal force acting on the material and pulling it towards the center as the

nozzle negotiates a radial toolpath. This explanation can be further verified by comparing the material velocity magnitudes (shown in arrows in Figure 4) under different ξ, values. Even though the right segment of the filament is underfilled, the high-velocity zone (shown in red arrows and circled in white) still exists. Due to the reduction in centripetal force with the increase in ξ, it can be seen that the region of the high-velocity zone also increases. The high-velocity zones also indicate that more materials are pushed to the right segment of the filament, hence, improving the uniformity of material distribution. Using ϕ as the parameter to characterize mass distribution homogeneity, it was determined that the increase in ξ, from 1.00 to 1.15 improves mass distribution homogeneity as ϕ reduces from 1.35 to 1.23.

The influence of the nozzle aspect ratio on mass distribution is shown in Figure 5, where φ is ranged between 1.5 and 2.0. To achieve these aspect ratios, L was fixed at 30 mm, and W values at 15 mm and 20 mm were used. Arising from the conservation of mass, the layer thickness of the deposited filament is directly related to the nozzle width, i.e., a nozzle with smaller φ (or larger W) produces a larger layer thickness. This can be clearly observed in Figure 5, where the layer thickness for φ = 1.5 (Figure 5a) is larger than φ = 2.0 (Figure 5b). Furthermore, it is also apparent from the figures that a larger layer thickness (or smaller φ) results in an improved homogeneity of the filament as compared to the extrudate with a smaller layer thickness (or larger φ), i.e., as φ decreases from 2.0 to 1.5, ϕ changes from 1.25 to 1.21. Owing to the larger layer thickness, the filament weight is increased, increasing the force it exerts on itself to press the filament towards the base. As a result of this mechanism, the unfilled zone on the right segment of the filament deposited by the nozzle with φ = 1.5 is significantly reduced when compared to the filament that is deposited using a nozzle with φ = 2.0.

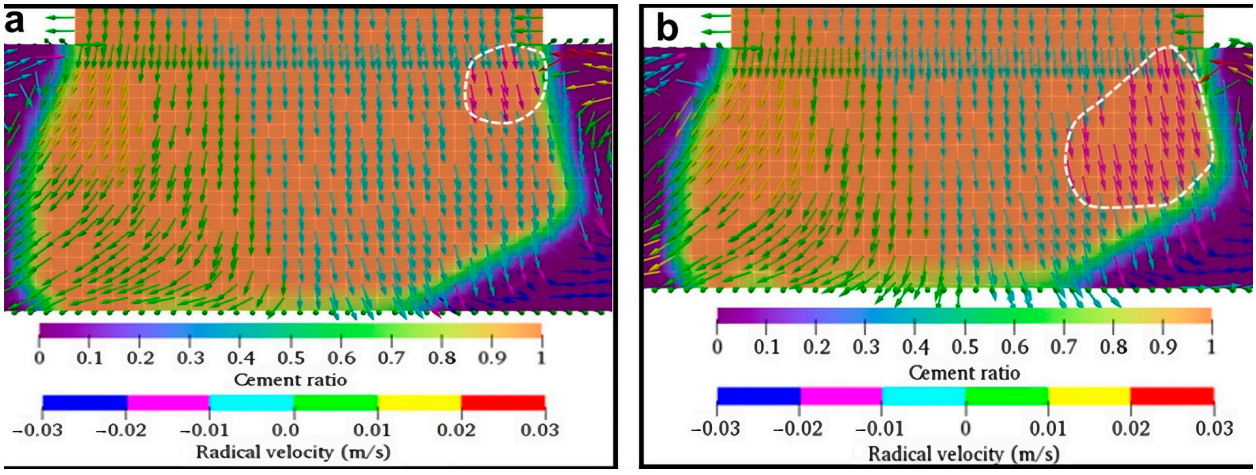

Figure 5. Cement ratio and velocity vector using a rectangular nozzle, R = 30 mm, ζ = 1.05, and φ of (**a**) 1.5 and (**b**) 2.

It can be concluded from the aforementioned analysis (Figures 4 and 5) that conventional rectangular nozzles are inadequate to provide uniform material distribution at corners. When the R value is fixed, the non-homogeneity of the material distribution increases as ζ and φ increase, which is also consistent with the findings reported in Ref. [8]. This inadequacy of the rectangular nozzles in providing a uniform material distribution stems from the inertia-induced centripetal force pulling the material towards the center of the radial toolpath. To overcome this issue of non-homogeneity, it is then required to (1) increase the material deposition rate at the outer segment of the filament to compensate for the low mass distribution in the underfilled zone and (2) to decrease the material deposition rate at the inner segment of the filament to reduce the mass distribution in the overfilled zone. In this regard, a trapezoidal nozzle can be employed to control the material deposition rate across the filament to enhance the extrudate uniformity. A top-

view schematic of a trapezoidal nozzle is shown in Figure 6a, where L_i and L_o represent the parallel sides of the trapezium, with L_i having a shorter width and L_o having a longer width; W denotes the width of the trapezium at the mid-point and L is the length of the trapezium. For the case where the length ratio (LR) of the trapezoidal nozzle is greater than 1, where $LR = L_o/L_i$, and considering that material exit velocity (V_i) is uniform, it will result in more material being deposited on the outer segment of the filament to compensate for the underfilled zone.

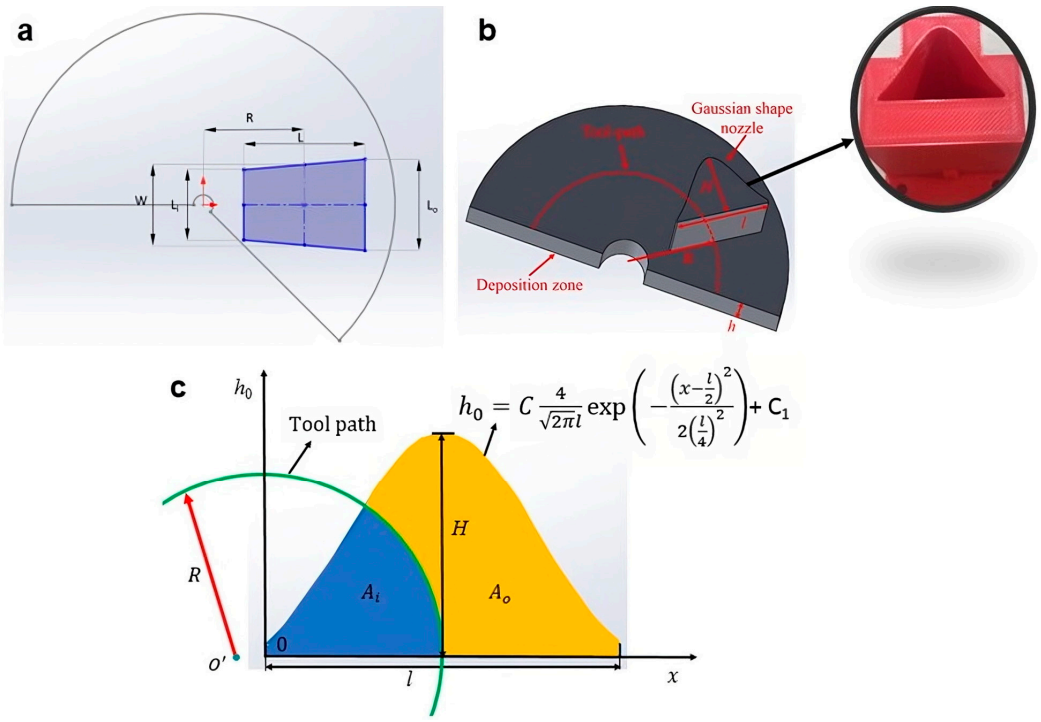

Figure 6. (**a**) Schematic of trapezoidal nozzle, (**b**) image of Gaussian nozzle and illustration of cementitious material deposition, and (**c**) cross-sectional profile of the Gaussian-shaped nozzle.

To validate this hypothesis, additional numerical simulation was performed on a trapezoidal nozzle of $LR = 1.2$ and $\varphi = 2.5$ and the filament mass distribution was compared with a rectangular nozzle of the same φ value, i.e., $\varphi = 2.5$. Here, $LR = 1.2$ is selected to compensate for the material distribution inhomogeneity of the rectangular nozzle based on the simulation result. A comparison of the material mass distribution is depicted in Figure 7, where $LR = 1.0$ (Figure 7a) represents the rectangular nozzle. It can be clearly observed from the comparison of the two figures that the unfilled zone at the outer segment of the filament (blue region underneath the material) is significantly reduced when the trapezoidal nozzle is used. In all, the trapezoidal nozzle achieves a lower ϕ value of 1.24 as compared to the ϕ value of 1.29 for the rectangular nozzle. To further improve the homogeneity of the deposited material, trapezoidal nozzles with larger LR ratios should be used. The increase in LR introduces more materials on the outer segment of the filament and has the advantage of gravity-induced filament filling (see explanation in Figure 5 in the previous paragraph for the detailed illustration of this mechanism). However, when the LR becomes too large and the L_i value reduces significantly, nozzle clogging can be a concern. Furthermore, with one control parameter, i.e., the LR ratio, to vary the extrudate material distribution, improving material homogeneity below an ϕ value of 1.20 for small toolpaths can be challenging.

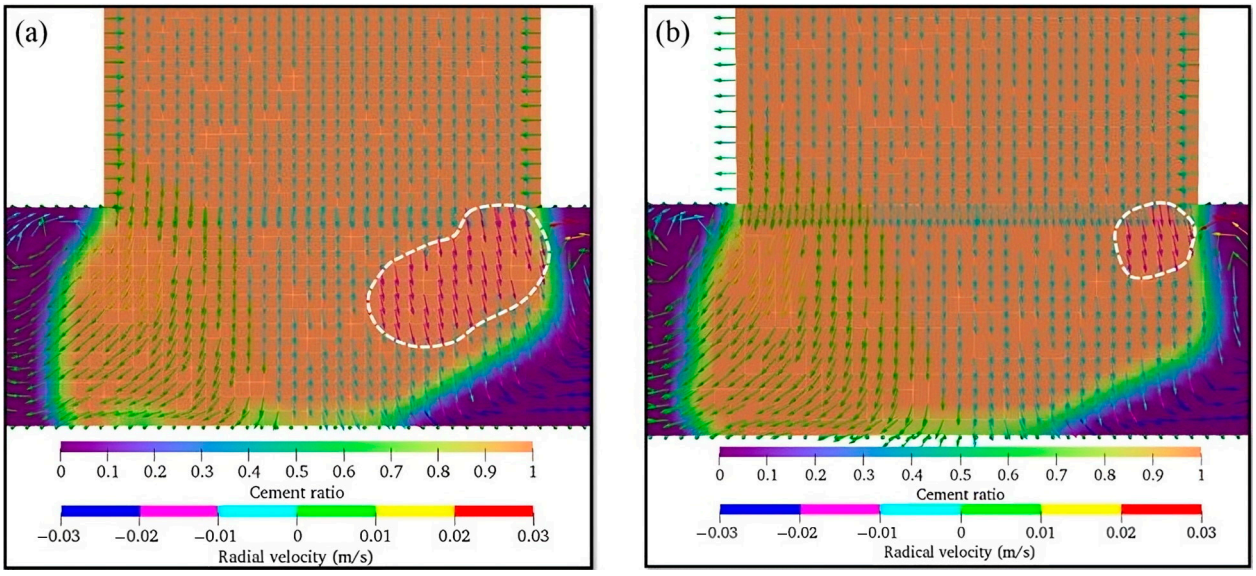

Figure 7. Cement ratio and velocity vector using a trapezoidal nozzle of *LR* of (**a**) 1.0 and (**b**) 1.2.

To overcome the drawback of the trapezoidal nozzle, we further explored the utilization of Gaussian-shaped nozzles. As shown in Figure 6b,c, the width of this nozzle varies with the nozzle length and takes the form of a Gaussian distribution. The Gaussian profile can be characterized by Equation (5) where h_0 denotes the nozzle length, and H and l are the maximum nozzle length and width of the Gaussian-shaped nozzle, respectively. In addition, μ and σ are the mean and standard deviations, and C and C_l are constants which can be used as fitting parameters to realize the desired Gaussian profile. Such a nozzle shape has several advantages over rectangular and trapezoidal nozzles. Firstly, studies have shown that the Gaussian nozzle produces a lower Poiseuille number when compared to rectangular and trapezoidal nozzles [15]. This reduces the tendency of nozzle blockage due to high differential pressure [16] and enables a continuous and smooth flow of materials. Secondly, the four fitting parameters of Equation (5) also increase the design freedom for the optimized Gaussian profile to achieve the required mass distribution when compared to the trapezoidal nozzle. For consistency of comparison, C and C_l in Equation (5) are set at the values of 432 and -1.9, respectively; $\mu = l/2$ and $\sigma = l/4$ are chosen in Equation (5), such that the cross-section area is approximately the same as the rectangular and trapezoidal nozzles. The cross-section of the fitted curve is shown in Figure 6c.

Figure 8 shows the comparison of the material mass distribution of the filament extruded and deposited from the various nozzles at $\xi = 1$. It can be seen that the mass distribution of the filament is clearly more uniform ($\phi = 0.98$) when the Gaussian-shaped nozzle is used, and there are no unfilled and underfilled zones. In contrast, an unfilled zone still exists when the trapezoidal nozzle is used. As shown in Figure 8c, the boundary of the toolpath is skewed towards the left side of the Gaussian profile, such that A_i is less than A_o. This allows more materials to be deposited on the outer segment of the filament to compensate for the centripetal effect. Furthermore, this outer segment also has a large maximum nozzle width (H) which increases the material mass and assists in pushing the filament towards the base, eliminating the unfilled zones.

$$h_0 = C\frac{1}{\sqrt{2\pi}\sigma}\exp\left(-\frac{(x-\mu)^2}{2(\sigma)^2}\right) + C_1 \quad (5)$$

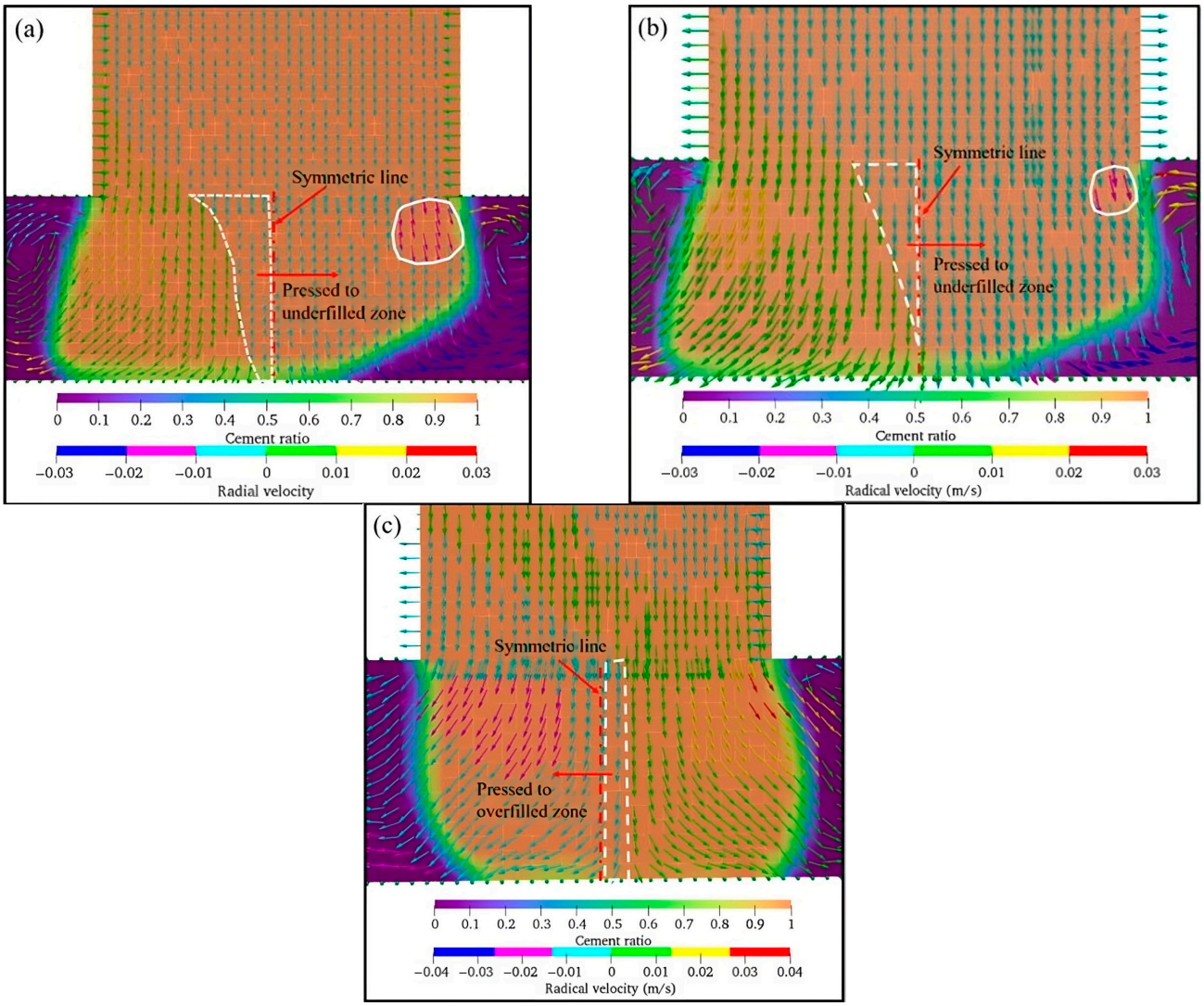

Figure 8. Cement ratio and velocity vector with R = 30 mm, ζ = 1.0, using (**a**) rectangular, (**b**) trapezoidal, and (**c**) Gaussian-shaped nozzles.

4. Conclusions

In this study, the mass distribution of 3D-printed cementitious material during the extrusion and deposition process and under a small radial toolpath was critically examined. From numerical simulation and analysis of the material deposition characteristics from standard rectangular nozzles, we identified the dominant mechanisms influencing the mass distribution of the materials and determined the inadequacies of these nozzles in attaining homogeneous mass distribution. Based on these observations, two new nozzle geometries, i.e., trapezoidal and Gaussian-shaped nozzles, were rationally proposed to compensate for the underfilled and unfilled zones and to take advantage of the gravity-induced filament filling mechanism. From the modelling results, it can be concluded that both trapezoidal and Gaussian-shaped nozzles achieved improved homogeneity of the filament compared to the rectangular nozzle, with the Gaussian-shaped nozzle demonstrating better filament uniformity. For the most extreme cases studied in this paper, the material distribution unevenness can be reduced from 1.35 to 1.23 and 0.98 after adopting trapezoid and Gaussian-shaped nozzles, indicating improvements of 34.3% and 94.2%, respectively. This work not only outlines the methodology for improving the quality of corner and curved features in 3DCMP but also introduces a new strategy which can be adopted for other extrusion-based fabrication techniques with high material inertia.

Author Contributions: Conceptualization, M.L., Z.L. and T.N.W.; methodology, M.L., Z.L. and J.Y.H.; software, M.L. and Z.L.; formal analysis, M.L., Z.L. and J.Y.H.; investigation, M.L., Z.L. and J.Y.H.; writing—original draft, M.L. and J.Y.H.; writing—review and editing, M.L., Z.L., J.Y.H. and T.N.W.; supervision, J.Y.H. and T.N.W.; project administration, T.N.W.; funding acquisition, T.N.W. All authors have read and agreed to the published version of the manuscript.

Funding: This research is supported by the National Research Foundation, Singapore, Prime Minister's Office, Singapore under its Medium-Sized Centre funding scheme, Singapore Centre for 3D Printing, Chip Eng Seng Corporation Ltd., CES_SDC Pte. Ltd., and CES_INNOVFAB Pte. Ltd.

Acknowledgments: The authors acknowledge the support of all undergraduate students and administrative and technical staff who were involved in this research.

Conflicts of Interest: The authors declare no conflict of interest.

References

1. Panda, B.; Unluer, C.; Tan, M.J. Extrusion and rheology characterization of geopolymer nanocomposites used in 3D printing. *Compos. Part B Eng.* **2019**, *176*, 107290. [CrossRef]
2. Chua, C.K.; Leong, K.F. *3D Printing and Additive Manufacturing: Principles and Applications (with Companion Media Pack) of Rapid Prototyping Fourth Edition*; World Scientific Publishing Company: Singapore, 2014.
3. Chua, C.K.; Leong, K.F.; Lim, C.S. *Rapid Prototyping: Principles and Applications (with Companion CD-ROM)*; World Scientific Publishing Company: Hackensack, NJ, USA, 2010.
4. Paul, S.C.; van Zijl, G.P.; Tan, M.J.; Gibson, I. A review of 3D concrete printing systems and materials properties: Current status and future research prospects. *Rapid Prototyp. J.* **2018**, *24*, 784–798. [CrossRef]
5. Commial, R.; Serdeczny, M.P.; Pedersen, D.B.; Spangenberg, J. Motion planning and numerical simulation of material deposition at corners in extrusion additive manufacturing. *Addit. Manuf.* **2019**, *29*, 100753.
6. Bos, F.; Wolfs, R.; Ahmed, Z.; Salet, T. Additive manufacturing of concrete in construction: Potentials and challenges of 3D concrete printing. *Virtual Phys. Prototyp.* **2016**, *11*, 209–225. [CrossRef]
7. Ngo, T.D.; Kashani, A.; Imbalzano, G.; Nguyen, K.T.; Hui, D. Additive manufacturing (3D printing): A review of materials, methods, applications and challenges. *Compos. Part B Eng.* **2018**, *143*, 172–196. [CrossRef]
8. Liu, Z.; Li, M.; Tay, Y.W.D.; Weng, Y.; Wong, T.N.; Tan, M.J. Rotation nozzle and numerical simulation of mass distribution at corners in 3D cementitious material printing. *Addit. Manuf.* **2020**, *34*, 101190. [CrossRef]
9. Lao, W.; Li, M.; Wong, T.N.; Tan, M.J.; Tjahjowidodo, T. Improving surface finish quality in extrusion-based 3D concrete printing using machine learning-based extrudate geometry control. *Virtual Phys. Prototyp.* **2020**, *15*, 178–193. [CrossRef]
10. Liu, Z.; Li, M.; Weng, Y.; Qian, Y.; Wong, T.N.; Tan, M.J. Modelling and parameter optimization for filament deformation in 3D cementitious material printing using support vector machine. *Compos. Part B Eng.* **2020**, *193*, 108018. [CrossRef]
11. Chen, X.; Fang, G.; Liao, W.-H.; Wang, C.C.L. Field-Based Toolpath Generation for 3D Printing Continuous Fibre Reinforced Thermoplastic Composites. *Addit. Manuf.* **2022**, *49*, 102470. [CrossRef]
12. Cao, X.; Yu, S.; Cui, H.; Li, Z. 3D Printing Devices and Reinforcing Techniques for Extruded Cement-Based Materials: A Review. *Buildings* **2022**, *12*, 453. [CrossRef]
13. De Rosa, S.; Tammaro, D.; D'Avino, G. Experimental and Numerical Investigation of the Die Swell in 3D Printing Processes. *Micromachines* **2023**, *14*, 329. [CrossRef] [PubMed]
14. Lombardi, L.; Tammaro, D. Effect of Polymer Swell in Extrusion Foaming of Low-Density Polyethylene. *Phys. Fluids* **2021**, *33*, 033104. [CrossRef]
15. Nguyen, N.T.; Chan, S.H. Pattern Molding of Polymeric Flow Channels for Micro Fuel Cells. U.S. Patent US7736788B2, 15 June 2010.
16. Zareiyan, B.; Khoshnevis, B. Effects of interlocking on interlayer adhesion and strength of structures in 3D printing of concrete. *Autom. Constr.* **2017**, *83*, 212–221. [CrossRef]